Materials Science & Engineering C 85 (2018) 170–181

Contents lists available at ScienceDirect

Materials Science & Engineering C

journal homepage: www.elsevier.com/locate/msec

Simple fabrication of rough halloysite nanotubes coatings by thermal spraying for high performance tumor cells capture

Rui He[a], Mingxian Liu[a,*], Yan Shen[a], Rong Liang[b], Wei Liu[b], Changren Zhou[a]

[a] Department of Materials Science and Engineering, Jinan University, Guangzhou 510632, China
[b] Department of Breast Surgey, Guangzhou Red Cross Hospital, Jinan University, Guangzhou 510220, China

ARTICLE INFO

Keywords:
Thermal spray
Halloysite
Roughness
Tumor cells
Capture yield
Cytocompatibility

ABSTRACT

Here, we reported a fast, low-cost, and effective fabrication method of large-area and rough halloysite nanotubes (HNTs) coatings by thermal spraying of HNTs ethanol dispersions. A uniform HNTs coating with high transparence is achieved with tailorable surface roughness and thickness. Compared with normal cells, the tumor cells can be captured effectively with high capture yield by the HNTs coatings (expect HeLa cells), which is attributed to the enhanced topographic interactions between HNTs coating and cancer cells. HNTs coating formed from 2.5% ethanol dispersions shows the highest tumor cells capture yeild (90%), which is related to the appropriate roughness and anti-EpCAM conjugation. The capture yield of HNTs coating towards MCF-7 cells can be further improved to 93% within 2 h under dynamic shear using a peristaltic pump. The capture yield increases with the incubation time, and the flow rate with 1.25 mL/min leads to the maximum capture yield. The HNTs coatings are also effective for capture of tumor cells spiked in artificial blood samples and blood samples from patients with metastatic breast cancer. More than 90% targeted MCF-7 cells and very small amounts of white blood cells are captured by the anti-EpCAM conjugated HNTs coatings from a blood sample. HNTs are further loaded anticancer drug doxorubicin (DOX) and then thermally sprayed into coatings. The MCF-7 cells captured on DOX loaded HNTs coating display significant membrane rupture characteristic and only 3% cell viability after 16 h. The high capture efficiency of tumor cells by HNTs coating fabricated by the thermal spraying method makes them show promising applications in clinical circulating tumor cells capture for early diagnosis and monitoring of cancer patients. The high killing ability of the DOX loaded HNTs coating can also be designed as an implantable therapeutic device for preventing tumor metastasis.

1. Introduction

In recent years, unique physical and chemical properties of nanomaterials motivated worldwide interests to form nanostructured coatings. Prior literatures have shown that surface topological structure of materials has a significant effect on cell behaviors, such as adhesion, proliferation, differentiation, and migration. The nanorough surfaces have various biomedical applications such as tissue engineering transplant [1], biological signal detection [2], repairing and healing of skin wound [3], and so on. The rough surfaces formed by nanoparticles with or without ordered arrangement are believed to enhance the cell interactions [4–9]. For example, a chip based on graphene oxide rough surfaces took advantage of the increased surface area afforded by the nanosheets for highly sensitive and selective tumor cell capture [10]. A uniform multiscale TiO_2 nanorod array prepared by hydrothermal synthesis method can also provide a “multi-scale interacting platform” for tumor cell capture [11]. However, the preparation methods such as evaporative assembly bear the shortcomings such as complicated producing process, difficulty of preparation of large areas coating with uniform thickness, and high fabrication prices which become a bottleneck for their extensive applications [12].

Thermal spraying represents a simple, fast, and effective scale-up manufacturing methods for nanostructured coating with large area. Various types and multi-purpose surfaces can be fabricated by spray-coating, including super-hydrophobic coating [13], pH-sensitive self-healing anticorrosion coatings [14], functional metal oxide coating [15,16], large transparent chemically-converted graphene films [17], and so on. For example, thin grapheme film prepared by spray deposition on preheated substrate shows a low sheet resistance of 2.2×10^3 Ω/sq. and a high transmittance of 84%. Quantum dot coating prepared by thermal spraying has excellent morphology and compositional purity, which can be used as solar cells [18]. The nanostructured coating applied in biomedicine area must have high bioactivity and biocompatibility, in addition to low-cost raw material and repeatable

* Corresponding author.
E-mail address: liumx@jnu.edu.cn (M. Liu).

https://doi.org/10.1016/j.msec.2017.12.030
Received 14 July 2017; Received in revised form 9 September 2017; Accepted 28 December 2017
Available online 29 December 2017
0928-4931/

processing [19–24].

Halloysite clay, a kind of natural nanoparticles with tubular morphology, combines the advantages of unique surface characters, high dispersion ability, high adsorption ability, good biocompatibility, and low cost [25]. The halloysite is often in the form of tube, and is often referred to as halloysite nanotubes (HNTs). Typically, the length and the outer diameter of HNTs are in the range of 200–1500 nm and 50–70 nm. HNTs are commonly used as nanofiller for the production of high-performance polymer composites [26]. Recently, HNTs have been recognized as novel biomaterials. Studies have shown that inorganics such as HNTs can be used to utilize for the encapsulation and control release of chemical/gene drugs [27–29]. HNTs can prolong half-life of drugs, increase loading amount of drug, and improve sustained release performance of drugs [30–32]. For enzyme immobilization, the immobilized enzymes in the channels of HNTs exhibited thermal stability, excellent storage stability and reusability [33,34]. Addition of HNTs can also produce high strength tissue engineering scaffold, since HNTs can improve the mechanical and thermal stability of polymer scaffolds [35,36]. Also, HNTs can be used as hemostasis agent and wound repair materials. Previous studies showed that HNTs can decrease the clotting time at high concentration and increases the wound healing rate [37,38]. HNTs can also be utilized as biomineralization nanoreactor to form urease-catalyzed $CaCO_3$ to exhibit a metastable vaterite phase structure [39]. HNTs-coated plastic microtube showed enhanced tumor cell adhesion under flow [40–42]. In our previous study, ordered HNTs coating by evaporation-induced self-assembly has also shown high capture efficiency towards various tumor cells [43].

Here, a strategy to produce uniform HNTs coating with large areas was developed by a simple thermal spraying method. A series of HNTs ethanol dispersion was thermally sprayed on glass substrates. The relationships between the surface morphology of the coatings and the cell capture performances were investigated. To increase the capture yield of tumor cells, the experiments were performed under dynamic shear using a peristaltic pump. Also, the artificial blood samples with spiked tumor cells and blood sample from patients with metastatic breast cancer were used to determine the capture efficiency of the HNTs coatings. Finally, the HNTs biodevices were expanded to kill the tumor cells by loading of anticancer drug doxorubicin (DOX). The morphology and cell viability of the captured tumor cells were investigated. All these results indicate that the HNTs coating fabricated by thermal spraying can be developed as promising cancer detection and treatment device in clinical application.

2. Experimental

2.1. Materials

Halloysite clay was purchased from Guangzhou Runwo Materials Technology Co., Ltd., China. Before using, halloysite clay was crushed into powder and purified by centrifugation. Streptavidin (SA), biotinylated anti-human-EpCAM/TROP1 antibody (goat IgG), doxorubicin (DOX) were purchased from Sigma–Aldrich. Diamidino-2-phenylindole dihydrochloride (DAPI), fetal bovine serum (FBS), serum-free DMEM medium with high glucose, phosphate-buffered saline (PBS), Triton X-100, and 0.25% Trypsin-EDTA (Gibco, 1 ×) were purchased from Jiangsu KeyGEN BioTECH Co., Ltd., China. Alex Flour 488 Goat Anti-Mouse IgG was purchased from Thermo Fisher Scientific Inc. Butanedioic anhydride, 3-aminopropyltriethoxy silane (APTES), *N*, *N*-dimethyl formamide (DMF), N-Hydroxysuccinimide (NHS), 1-Ethyl-3-(3-dimethylaminopropyl) carbodiimide hydrochloride (EDC), and all other chemicals were purchased from Aladdin Industrial Corporation. Ultra-pure water was prepared by Milli-Q water system.

2.2. Preparation of HNTs coating

HNTs coating was prepared by thermal spraying method. Typically, 0.5 g, 1 g, 2.5 g, 5 g HNTs were dispersed in 100 mL of anhydrous ethanol by ultrasonic cell disruptor (scientz-IID, NingBo Scientz Biotechnology Co., Ltd., China) for 30 min. A clean piece of glass slide was placed on an 80 °C heating stage for 1–2 min, and then about 5 mL HNTs ethanol dispersion was poured into the pot of the spray gun. About 10 s with the rate of 3 mL/min was used to spray the glass slides for preparation of HNTs nano-coating. Spaying drying can rapid create silanol bonds between the silica surface and the HNTs. The robustness of the deposited coating was satisfied at the experiment condition. To decrease the hydrophilicity of HNTs, the HNTs coatings were soaked in 20 mL 4% (v/v) APTES in anhydrous ethanol solution for 1 h to stabilize HNTs coating during cell culture. The excess APTES was removed by washing the coating with anhydrous ethanol. Then the glass slides with HNTs coating were cut into 1 × 1 cm chunks for cell culture in 24-well plate. The blank glass slide was used as control.

2.3. Characterization of HNTs coatings

The transparency of the HNTs coatings was shot by a camera and the quantitative analysis was determined using ultraviolet spectrophotometer (UV-2550, Shimadzu Instrument Ltd., Suzhou China) from 350 nm to 1000 nm wavelength. The microstructure of the HNTs coatings was analyzed by field emission scanning electron microscopy (Ultra-55, Carl Zeiss Jena Ltd., Germany) at 5 kV. The HNTs coating surfaces were plated with a thin layer of gold before the observations. The surface morphology of the HNTs coatings was characterized using atomic force microscopy (AFM) with NanoScope IIIa controller (Veeco Instruments Inc.). The height distribution of HNTs coating, the quantitative analysis of root-mean-square roughness (R_q), and average roughness (R_a) were acquired by the NanoScope Analysis Software. The measured roughness of the surface was affected by spatial and vertical resolution and the radius of the cantilever tip (on the order of nanometers for the used silicon tip) of the instrument.

2.4. Cell culture

Mouse osteoblastic cell (MC3T3-E1), human liver cell (L02), human hepatoma cells (HepG2), human breast cancer cells (MCF-7), human cervical cancer cells (HeLa), human lung carcinoma cells (A549), metastatic murine melanoma cells (B16F10), and human prostate cancer cells (PC3) were purchased from the laboratory animal center of Sun Yat-sen University. All the cells were maintained in Dulbecco's Modified Eagle's medium (DMEM, Life Technologies) supplemented with 10% fetal bovine serum (FBS, Life Technologies), 1% penicillin (100 U·mL^{-1})/streptomycin (100 μg·mL^{-1}). All cell lines were maintained at 37 °C in a humidified atmosphere of 5% CO_2 in air as a monolayer culture in plastic culture flask (25 cm^2, Corning, NY, 14,831). The cells were grown to ~80% confluence before passaging with trypsin/ethylene-diaminetetraacetic acid (EDTA) (Life Technologies) incubation for 2–3 min.

2.5. Cell capture and characterization

The HNTs coatings were soaked in 75% alcohol solution for 2 h and washed with PBS for 3 times. Afterwards, they were exposed under ultraviolet light for 2 h. The HNTs coatings (1 × 1 cm) were placed into 24-well cell culture plates and then 1 mL cell suspension (1.0 × 10^4 cells·mL^{-1}) was added into each well. The cell culture plates were incubated in a cell incubator (37 °C, 5% CO_2, HF 100, Heal Force Bio-Miditech Ltd., China) for 1 h, 2 h, and 3 h, respectively. The coatings were then rinsed with PBS for 3 times to remove the cell culture medium. The cells captured by the coatings were fixed by paraformaldehyde solution (4 wt% in PBS) for 10 min and penetrated with Triton X-100 (0.2 wt% in PBS) for 10 min for cell staining. DAPI solution (5 μg·mL^{-1} in PBS) was used to stain the captured cells on the coating for 5 min and the cells were washed with PBS for 3 times to

remove excess DAPI. The captured cells were observed with a fluorescence microscopy (EVOS® FL Cell Imaging System, USA). At least 10 fluorescence images of captured cells on different regions of the coating were recorded at 50 × magnification. The numbers of captured cells were counted by Image J software (National Institutes of Health, USA). The capture yield was calculated by comparing the capture cell number with the initial number of cells added to each well (1×10^4 cells). The morphology of captured cells in the HNTs coatings was further analyzed by SEM. Before SEM observation, the cells were fixed with 2.5% glutaraldehyde in PBS buffer at room temperature for 2 h and dehydrated in ethanol at 30, 50, 70, 80, 90, 95, and 100% concentration for 15 min respectively. The samples were then freeze-dried at − 80 °C for 24 h and dealt with the high vacuum gold jetting. The morphology of cells were observed at 2.0 kV.

2.6. Bioconjugating with anti-EpCAM on the HNTs coatings

The surface was conjugated with antibody according to previous study [44]. Typically, the HNTs coatings were soaked in 10 μg·mL^{-1} SA solution in PBS at 4 °C overnight in order to make the adsorption of SA on HNTs. Afterwards, the coatings were washed for 3 times with PBS to remove free SA. Then the coatings were incubated with anti-EpCAM (10 μg·mL^{-1} in PBS) at room temperature for 2 h and rinsed by PBS for 3 times to remove the excess antibody. The coatings conjugated with anti-EpCAM were placed into 24-well cell culture plates and the capture process of cells was similar to the previous procedure.

2.7. Capture of tumor cells by HNTs coatings under dynamic shear condition

The HNTs coatings (length × width: 2.5 × 1.5 cm) were placed in a plexiglas box (the inside length × width × height: 2.5 × 1.5 × 1.0 cm) with removable lid and holes (diameter: Φ 2 mm) on the lid. 2 mL cell suspension (1.0×10^4 cells mL^{-1}) was added into the box. The device was connected to a peristaltic pump (BQ 80S, Baoding lead fluid technology Co., Ltd., China) through rubber pipes (inner diameter: Φ 1 mm). The flow rate was set as 0–5 mL·min^{-1} and the incubation temperature was 37 °C. The staining and counting process of cells was similar to the previous procedure. To study the captured cell morphology, the tumor cells were stained firstly by Alex Flour 488 Goat Anti-Mouse IgG for 300 μL for each well and then DAPI (10 μg·mL^{-1} concentration) for 300 μL. The fluorescence images were obtained by an inverted XDY-2 microscope (Guangzhou Yuexian optical instrument Co., Ltd., China).

2.8. Patients and healthy controls

The study was approved by the Ethics Committee from the Fourth Affiliated Hospital (Guangzhou Red Cross Hospital) of Jinan University. All peripheral blood was collected with the patients' written consent. Patients presented with a clear pathological diagnosis of breast cancer between November and December 2016. The patient's condition ranged from stage II to stage III. Patients were aged 33–92 years with an average age of 59.6 years. Preoperative physical examination and laboratory detections excluded other malignant tumors before removing the tumor tissue by lumpectomy. Healthy blood samples were collected from healthy volunteers.

2.9. Capture of tumor cells from artificial blood samples and blood samples of patients with metastatic breast cancer

2 mL peripheral blood was collected from healthy donator and preserved in blood collection tubes before use (containing EDTA). MCF-7 cells were firstly dyed by DAPI for 5 min before using. Different numbers of MCF-7 cells (10, 50, 100, 1000 and 10,000 per milliliter) were spiked artificially into the 1 mL blood sample (diluted by the same volume of DMEM). The solution samples with tumor cells were transferred to the circulating box (length × width × height: 2.5 × 1.5 × 1.0 cm) with HNTs coating conjugated with or without anti-EpCAM. After capturing for 2 h, the cells on the coating were rinsed by PBS and observed using a fluorescence microscope (XDY-2, Guangzhou Yuexian optical instrument Co., Ltd., China), and the number of the cells on the coatings was counted by Image J software.

2 mL diluted blood samples from patients with metastatic breast cancer were placed to the plexiglas box with HNTs coating conjugated with anti-EpCAM. The capture process was last for 2 h under 1.25 mL·min^{-1}. The HNTs coatings were then rinsed by PBS for several times. The cells were fixed and penetrated with 4% paraformaldehyde and 0.5% Triton X-100 for 10 min. Subsequently, PE-labeled anti-Cytokeratin 19 (CK19, a protein marker for epithelial cells), FITC-labeled leukocyte common antigen (anti-CD45, a marker for white blood cells) were used to specifically stain MCF-7 cells and white blood cells (WBCs) captured by HNTs coating. The cell nuclei were stained by DAPI. These cells were then imaged by an inverted fluorescence microscope.

2.10. Killing the captured tumor cells by DOX loaded HNTs coating

1 mg DOX was dissolved in 10 mL anhydrous ethanol firstly, and 250 mg HNTs were dispersed in the solution by ultrasonic treatment for 30 min. Then the solution was let overnight until the upper solution became colorless and transparent. The DOX loaded HNTs were evenly dispersed in the ethanol solution by shaking. The thermal spraying process for nano-coating was similar to the previous procedure. Then the HNTs-DOX coating was placed to plexiglas box with 1 mL MCF-7 cell suspension (1×10^4 cells·mL^{-1}) which linked to a peristaltic pump. After capturing for 2 h, the coating was rinsed by PBS for 3 times and moved to 6-well cell culture plates for culturing. The cells were incubated by adding new medium for different time to carry CCK-8 colorimetric assay at 450 nm. On the other hand, acridine orange (AO) and ethidium bromide (EB) double staining were used to detect apotosis of captured cells by the HNTs coatings with and without DOX.

3. Results and discussion

3.1. Thermal spraying for preparation HNTs coating

HNTs were evenly dispersed in anhydrous ethanol firstly, and the dispersion was atomized rapidly and sprayed from the nozzles of airbrush under the air pressure. When the dispersion was sprayed on hot glass slides, the alcohol was evaporated rapidly due to its low boiling point (78 °C). As a result, HNTs were pinned on the glass slides via Van der Waals force and hydrogen bond interactions, which formed a uniform rough coating composed of HNTs. The preparation process of HNTs coating and the conjugation with antibodies to capture tumor cells are shown in Fig. 1(A). The appearance of HNTs coating on glass slides is shown in Fig. 1(B).

The coatings formed at relatively low HNTs concentration (0.5% and 1%) are almost transparent. With increasing the concentration of the HNTs dispersion, the transparency of coating is getting worse. As the concentration of the HNTs dispersion reaches to 5%, the highest transparency of the HNTs coating declines to 40%. So, the HNTs dispersion concentration has a significant effect on the light transmission of the coating. However, the coating is semitransparent even with high HNTs concentration, which is convenient for observing the captured cells by staining. To illustrate the microstructure of the HNTs coating, SEM was performed on the samples (Fig. 2). The SEM photos of the coatings formed by spraying of different HNTs dispersion are in accordance with optical microcopy result above. A dense layer of HNTs is formed on the coating with arbitrary tubes arrangement. The surface roughness of the coating increases with the concentrations of HNTs dispersion. It also can be seen there are more traps formed by large

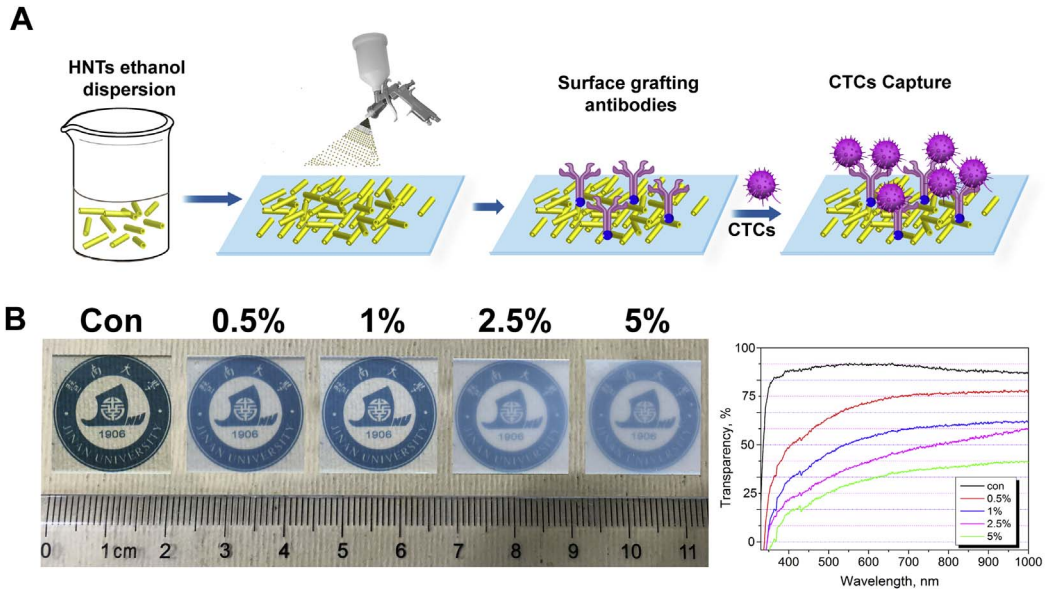

Fig. 1. The schematic illustration of preparation of HNTs coatings and conjugation with antibodies to capture tumor cells (A). The photograph of HNTs coatings formed from different concentrations of HNTs ethanol dispersion and light transmittance of the different HNTs coatings (B).

number of nanotubes for the 2.5% and 5% HNTs coating. Previous studies suggested that the surface roughness of coating have significant effects on the interactions with cells [45–47].

AFM was further applied to determine the influence of the dispersion concentration on the 3D morphology and surface roughness (Fig. 3(A)). The roughness increases with the concentration of HNTs dispersion, which is consistent with SEM results. The surface height distribution of the HNTs coating determined by AFM is shown in Fig. 3(B). The average height of the HNTs coating increases from 0.49 μm to 1.64 μm with increase in the HNTs dispersion concentration. And likewise, the roughness increases with the concentration of HNTs dispersion (Fig. 3(C)). The HNTs coating formed from 0.5% HNTs dispersions shows R_q and R_a of 140 nm and 109 nm respectively, whereas it is 314 nm and 251 nm for the 5% HNTs dispersion. So, the roughness of the HNTs coating by thermal spraying can be tailored by controlling the HNTs dispersion concentration. Suitable roughness of coatings is favorable for cell attachment [48,49].

3.2. Capture of tumor cells by the HNTs coating under static state

Thermal spraying of HNTs on the glass substrate is a simple process to prepare uniform HNTs coating with controllable roughness. The rough HNTs nano-coating can be used as substrate for capture of circulating tumor cells (CTCs) from cancer patient's blood. To investigate the effect of surface roughness of HNTs coating on the cell capture yields, a series of simulation experiments to capture normal cells or tumor cells from cell culture medium were performed with smooth glass surface as control. Fig. 4(A) shows the fluorescence images of DAPI-stained MC3T3-E1 cells captured on smooth glass slide and 2.5% HNTs coatings for 1, 2, 3 h. It can be seen that the MC3T3-E1 cell numbers captured by both the two surfaces increase with the capture time. When compared with the two surfaces, they have similar capture

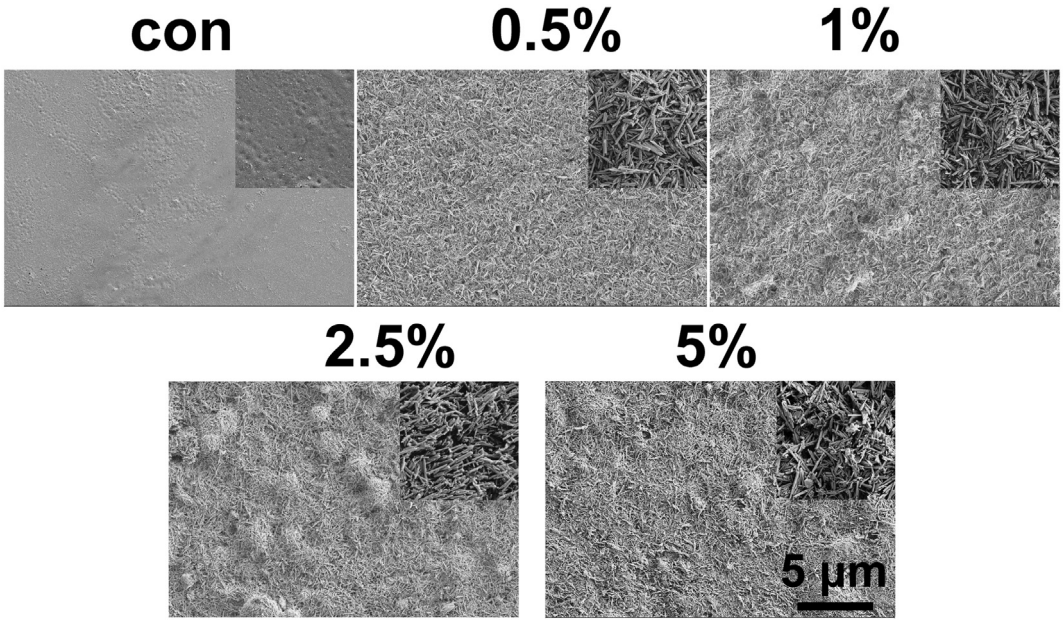

Fig. 2. SEM images of the different HNTs coatings (inset shows the enlarged SEM photos).

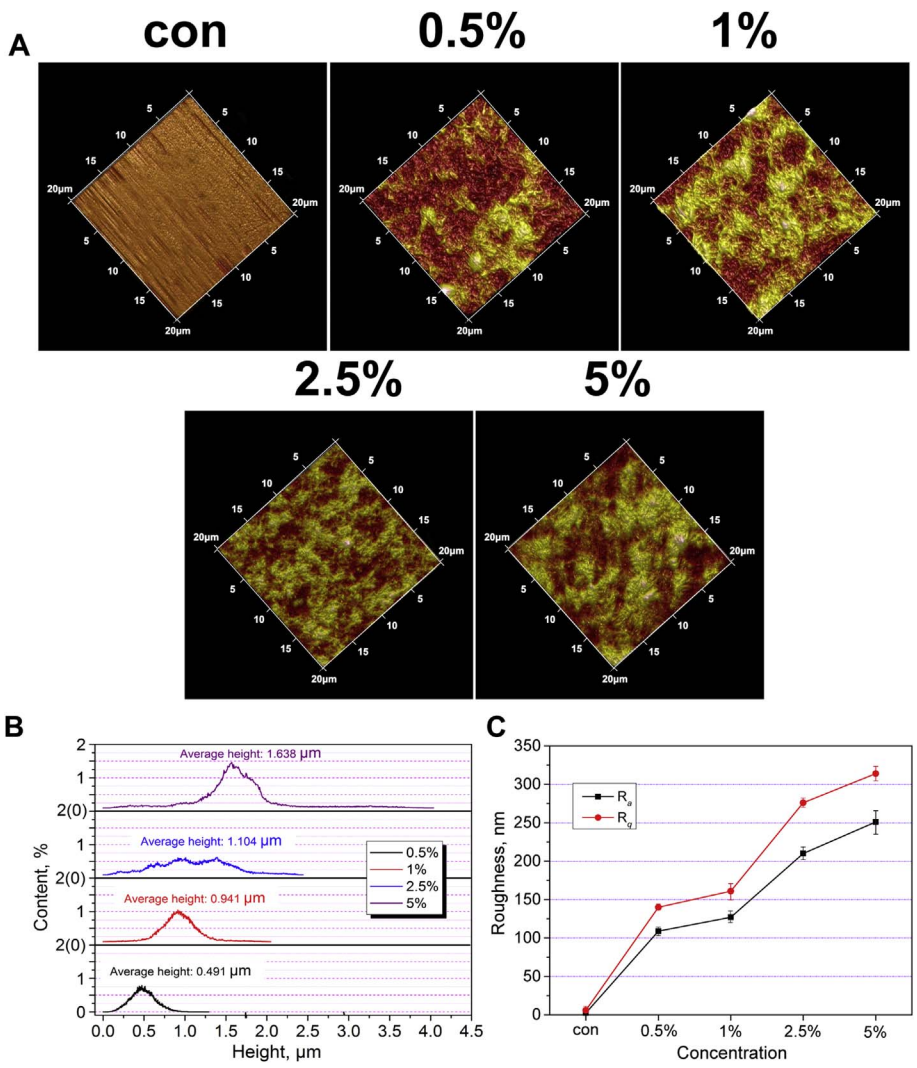

Fig. 3. AFM images of the different HNTs coating (A). The surface height distribution of the different HNTs coatings (B). The quantitative analysis of R_q and R_a of the different HNTs coatings (C).

yield to MC3T3-E1 cells in the first hour. After 3 h of incubation, the 2.5% HNTs coating surface has a slightly higher capture yield (27%) than the smooth glass surfaces (17%). By comparing the capture performance of MCF-7 cells (Fig. 4(B)), the HNTs coating surfaces can capture much more cells than that of smooth glass surfaces. On the other hand, the HNTs coating surfaces can capture much more MCF-7 cells than the MC3T3-E1 cells.

The number of cells captured on the surfaces with same areas was counted via Image J software to quantify the capture yield (Fig. 5(A)). All the HNTs surfaces show capture yield of MC3T3-E1 cell in the range of 20%–27% after 3 h incubation which is slightly higher than that of the control group (17%). The 2.5% content of HNTs coating surface has the highest capture yield compared to others, which may be attributed to the proper surface roughness of the coating. Fig. 5(B) shows the relationship between MCF-7 cells capture yield with incubation time on the blank glass and different HNTs coatings with different incubation time. It can be seen that the capture yield increases with the incubation time. The capture yield increases significantly especially after 2 h and the capture yield by HNTs coating surfaces are all higher than that on the blank glass surface. After 3 h of incubation, the 2.5% HNTs coating surface has the highest MCF-7 cell capture yield compared to others similarly. The capture yield towards MCF-7 can reach to 83% ± 3% for the 2.5% HNTs coating, while the control group is only 28.5% ± 2%. A variety of normal cells (MC3T3-E1, L02) and tumor cells (MCF-7, HepG2, A549, HeLa, PC3, and B16F10) were further used to investigate the capture yield for the 2.5% HNTs coating surface (Fig. 5(C)). It also can be seen that the HNTs coatings show high capture yield for most of the tumor cells (except HeLa cells) and relatively low capture yield for the normal cells. Some studies have also shown that rough coating has low capture yield towards to HeLa cells [50], which is due to the different cell surface structure of HeLa cells. Among the used cells, the capture yield of B16F10 and MCF-7 cells by the 2.5% HNTs coating surface without antibody conjugation reaches to 85% ± 2% and 83% ± 3% respectively after 3 h capture. In contrast, the capture yields of the MC3T3-E1, L02, and HeLa are less than 30%. The different capture yields of cells are related to both the surface roughness of HNTs coating and the cell surface structures which will be shown in the following section.

The surfaces with different roughness have a significant effect on the cell morphology [51,52]. The morphology of the captured cells was investigated by SEM (Fig. 6(A), (B)). Compared with smooth glass surface, the cells are easier to grasp on the HNTs coating surface as there are a large number of micropapilla formed by the HNTs aggregates. Compared with MC3T3-E1 cells, the MCF-7 cells have more microvilli and pseudopodia. So, it is more beneficial to adhesion of MCF-7 cells on the rough HNTs coating. It can be seen that the microstructure of the cells on the smooth and rough surface is different from the Fig. 6(A) and (B). It has been shown that normal cell-to-substratum adhesion is accompanied by the flattening and spreading of cytoplasm in the MC3T3-E1 group. While for MCF-7 cells, the adherent cancer cells appear as spheres attached to substrate by filopodia in smooth glass slide or as spheres slightly flattened by the spreading of

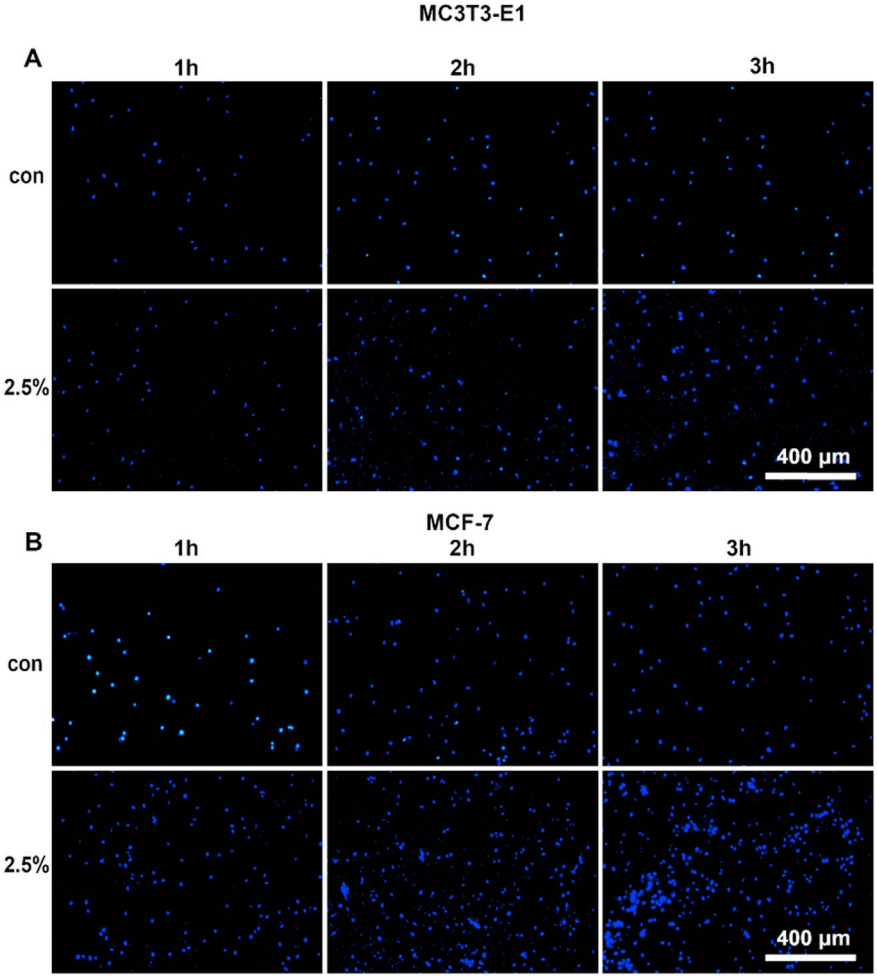

Fig. 4. The DAPI fluorescence microscopy images of captured cells of MC3T3-E1 (A) and MCF-7 (B) on the blank glass and HNTs coating.

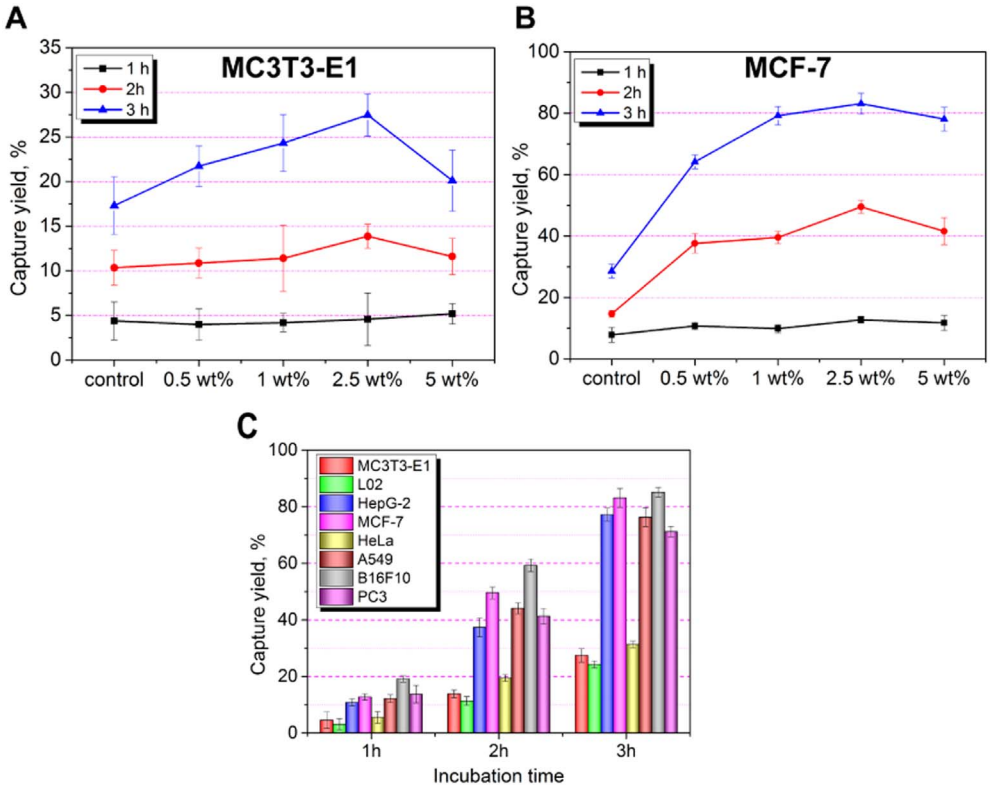

Fig. 5. The capture yield of MC3T3-E1 (A) and MCF-7 (B) on the blank glass and different HNTs coatings with different incubation time. The capture yield of different cells on the HNTs coatings formed by 2.5% HNTs dispersion with different incubation time (C).

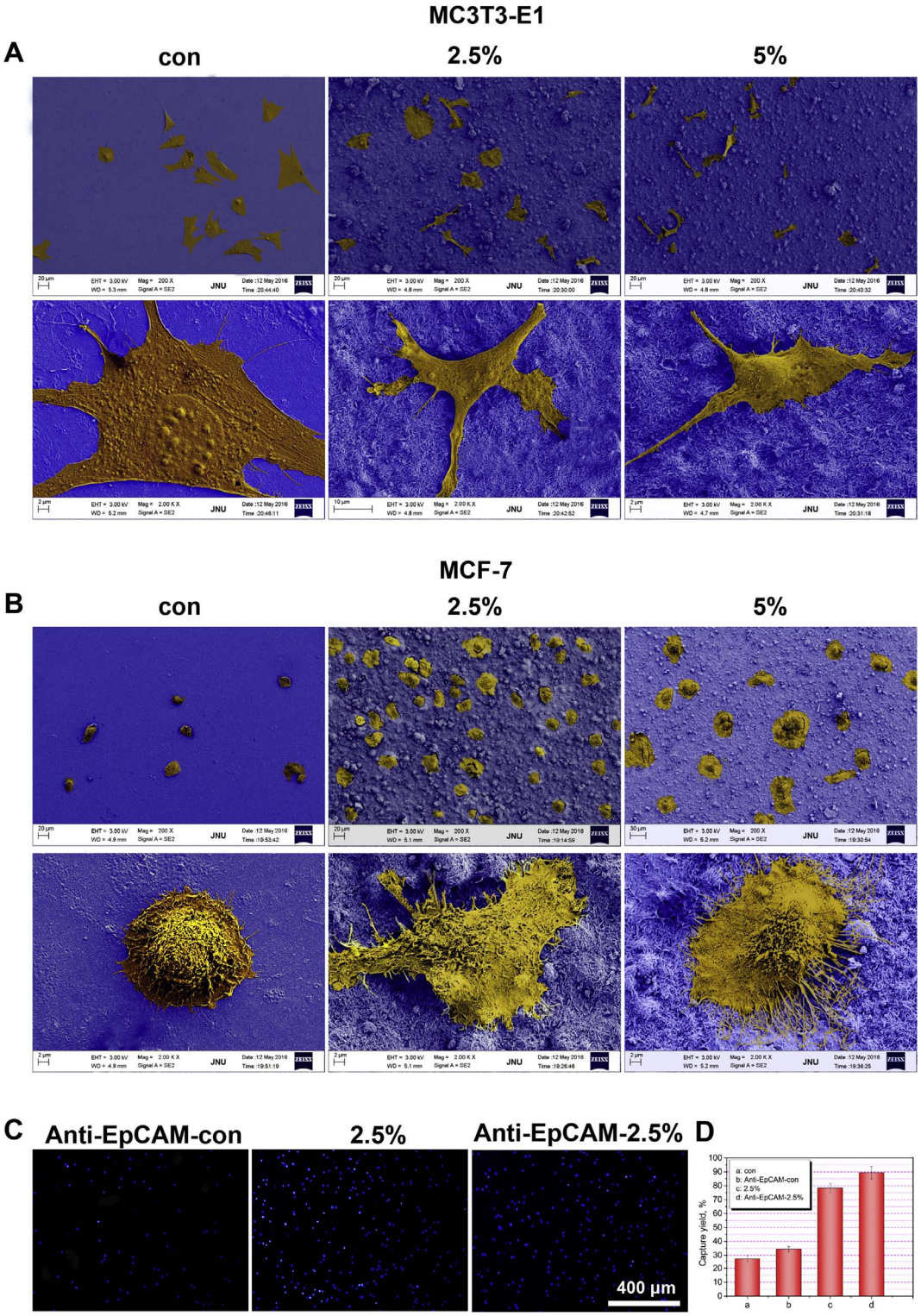

Fig. 6. SEM images of the microstructure topography of the MC3T3-E1 cells (A) and MCF-7 cells (B) on smooth blank glass and HNTs coatings (the images were artificially stained showing the cells and the substrates). The DAPI stained fluorescence microscopy images of captured MCF-7 cells on the smooth glass and 2.5% HNTs coating without and with anti-EpCAM conjugation (C). MCF-7 capture yield on different surfaces for 3 h (D).

cytoplasm in the rough HNTs coatings. One of the major differences between cancer cells and normal cells is the surface character. Cancer cells do not adhere to each other as firmly as normal cells do and hence they have the ability to metastasize or spread to other tissues of the body through the blood or lymph fluid. Researchers found that cancer cells had many more microvilli and pseudopodia than the normal cells in their surfaces. Therefore, the surface areas and the surface roughness of the cancer cells are greater than those of normal cells [53,54] So, the different surface roughness may be a common specialty between cancer cells and normal cells. The increased surface area and roughness of cancer cells may be related to the increased cell-matrix interactions and capture yield in the present systems. It can be seen that MCF-7 cells are fully extended pseudopodia attached to the rough HNTs coating surface. In contrast, the MCF-7 cells on the smooth glass surface are rare

and exhibit a rounded conformation with few extended pseudopodia and microvilli. Many studies showed that nanorough surfaces can stimulate the production of extracellular matrix (ECM) secreted [55,56]. A large number of ECM makes MCF-7 cells attach well on the rough HNTs coating surface. As shown in Fig. 6(B), the stained MCF-7 cell outgrew many long protrusions which connects the convex substance formed by HNTs. MCF-7 cells are more likely to adhere to the rough HNTs coating surface rather than smooth glass surfaces, which results in that the rough HNTs coating surface can grasp much more MCF-7 cells than smooth glass surfaces.

Surfaces conjugated with specific antibody or protein can attract more cells to be adhered [44,57]. EpCAM is expressed exclusively in epithelia and epithelial-derived neoplasms and not found in non-epithelial cells such as white blood cells (WBCs), so anti-EpCAM is always used as diagnostic marker for various cancers. The blank glass surface and HNTs coating surface were conjugated with anti-EpCAM to investigate the capture yeild of MCF-7 cells (Fig. 6(C)). It can be seen that the conjugation of anti-EpCAM on both smooth glass surface and HNTs coatings show much higher capture yield than those without antibody. After 3 h incubation, the capture yield of MCF-7 cells by the 2.5% HNTs coating conjugated with anti-EpCAM reaches up to 90% ± 2% which is much higher than that of unmodified HNTs coating (80% ± 3%) and the smooth glass surface conjugated with anti-EpCAM (35% ± 1%). This further confirms that the topology and surface chemistry of HNTs coating can improve the adhesion of tumor cells.

3.3. Capture of tumor cells by the HNTs coating under dynamic shear condition

In order to simulate blood circulation process of human body for capture of rare CTCs in cancer patients, a circulating device was built to test the capture yield towards tumor cells of HNTs coating under dynamic shear condition (Fig. 7(A)). The dynamic shear was expected to further increase of the capture yield of tumor cells by nano-surfaces [58,59]. Fig. 7(B) shows capture yield towards MCF-7 cell by 2.5% HNTs coating surface for 2 mL medium spiked with 1×10^4 MCF-7 cells with different flow rate by peristaltic pump for 2 h. It can be seen that when the flow rate is set as 1.25 mL·min^{-1}, the device exhibits the highest capture yield (79% ± 4.5%) which is comparable to the capture yield for 3 h without shear. The shear process with appropriate flow rate can increase the contact opportunity between the MCF-7 cells and rough HNTs coating surface, which consequently leads to more cells captured by the HNTs rough surfaces. When the flow rate is too fast, for example 5 mL·min^{-1}, the capture yield is only 1.3% ± 0.5%. This is due to that the MCF-7 cells can be washed away before adhering to the HNTs coating [60]. It should be noted that the volume of the blood sample for CTCs detection is only 2 mL, which is much less than that in human body. So, we selected the maximum flow rate of 5 mL·min^{-1} which is lower than the blood flow rate in human body (~15 cm/s). The small blood sample amount is used because of the conveniences for the clinic blood sampling from cancer patients. Fig. 7(C) compares the capture yield towards MCF-7 cell by different HNTs coating surfaces at a flow rate of 1.25 mL·min^{-1}. Similar to previous results, the 2.5% HNTs coating surface has the highest capture yield (79% ± 4.5%). This is related to that the 2.5% HNTs coating has the most suitable roughness ($R_a \approx 200$ nm) to capture tumor cells. From the SEM result above, there are many traps or bulge formed by nanotubes for the 2.5% coating. Surface roughness of substrates has significant effects on the interactions with cells. The rough HNTs coating surface can acquire higher capture yield under dynamic shear condition for 2 h. However, the smooth glass surface under dynamic shear condition exhibits much lower capture yield than that at static condition. So the roughness of the surfaces plays a critical role for determining the capture yield. Fig. 7(D) compares capture yield towards MCF-7 cells by 2.5% HNTs coating surface for different time at a flow rate of 1.25 mL·min^{-1}. The capture yield increases with the time. For 0.5 h, the capture yield of 2.5% HNTs coating surface to MCF-7 and B16F10 is only 2.8% ± 0.2% and 3.14% ± 0.75% respectively, while the capture yield is increased to 78% ± 3% and 83% ± 5% after 2 h respectively.

The morphologies of the MCF-7 cells captured by different HNTs coating surfaces after 2 h were investigated by fluorescence microscope via staining the cell with DAPI and Alex Flour 488 Goat Anti-Mouse IgG (Fig. 7(E)). The spreading areas of the cells are relatively large on the rough HNTs coating surface. The cells captured by 2.5% and 5% HNTs coatings have more microfilament in the microvilli and pseudopodia compared with those on others. The cytoskeletal intermediate filaments appear to impart tensile strength to the cell cytoplasm, which leads to that the cells turn from circular to irregular or polygonal in shape [61]. The large number of pseudopodia and microvilli spread from cytomembrane makes the cells be trapped in the rough HNTs coating. Fig. 7(F) and (G) are the DAPI stainned fluorescence microscopy images of the MCF-7 cells captured by different coating surfaces under dynamic shear condition for 1 h and then standing for another 2 h. And likewise, the 2.5% HNTs coating has the highest capture yield (86% ± 4%), which is slightly higher than that in static capture for 3 h (83% ± 3%). This further signifies the shear for the improved interactions between cells and rough surfaces. Fig. 7(H) shows the DAPI stained fluorescence microscopy images of captured MCF-7 cells on the smooth glass and 2.5% HNTs coating conjugated without and with anti-EpCAM for 2 h at a flow rate of 1.25 mL·min^{-1}. Fig. 7(I) shows the cell numbers counted via Image J software to quantify their cell capture efficiency. It can be seen that the anti-EpCAM conjugated HNTs surface can capture more tumor cells than the raw HNTs coating surface. The highest capture yield (93.5% ± 2.4%) can be obtained by 2.5% HNTs coating conjugated with anti-EpCAM for 2 h at a flow rate of 1.25 mL·min^{-1}.

The HNTs coating was further used to capture the tumor cells spiked in peripheral blood samples. The artificial whole blood samples were prepared by spiking healthy human blood with MCF-7 cells dyed by DAPI at concentrations of approximately 10, 50, 100, 1000, and 10,000 cells·mL^{-1}. The 2 mL solution samples with tumor cells were transferred to the circulating box for capturing 2 h under shear. The capture yield of raw HNTs coating ranges from 77% ± 3% to 83% ± 2.5%, while the anti-EpCAM conjugated rough HNTs coatings exhibit from 87% ± 3% to 93% ± 4% of capture yield towards targeted MCF-7 cells (Fig. 8(A)). The HNTs coating conjugated with anti-EpCAM can capture rare tumor cells from the blood sample, but very small amounts of white blood cells are captured by the coating. 50 MCF-7 cells were then added to 2 mL peripheral blood from healthy people and transferred to the circulating box for capturing 2 h at a flow rate of 1.25 mL·min^{-1}. DAPI stained fluorescence microscopy image shows that the volume of the WBCs is much smaller than MCF-7 cells and the number of WBCs is less than 2 cells per 1 mm^2 area of HNTs coating (Fig. 8(B)). Fig. 8(C) shows the three-color immunofluorescence fluorescent images of the captured cells by the HNTs coating from the artificial whole blood samples. As the MCF-7 cells can be dyed by PE-labeled anti-Cytokeratin (CK, a protein marker for epithelial cells) to red [62] (excitation peak wavelength 565 nm), while FITC-labeled anti-CD45 (a marker for WBCs) can be used to dyed the WBCs to green [63] (excitation peak wavelength 490 nm) and DAPI was used for nuclear staining (excitation peak wavelength 340 nm). The MCF-7 cells (red cytoskeleton and blue nuclei) can be identified from non-specifically captured WBCs (green cytoskeleton and blue nuclei).

2 mL fresh blood samples obtained from patients with metastatic breast cancer ($n = 6$) were further used to investigate the CTCs capture ability of HNTs coatings conjugated with anti-EpCAM (Fig. 8(D) and (E)). The captured rare CTCs number by the HNTs coating in the blood sample can reach as high as 5 in 1 mL blood, while only 220 WBCs are captured in 1 mL blood sample. The capture yield of WBCs is calculated as less than 0.0055% (4–11 × 10^6 WBCs in 1 mL blood). Therefore, the anti-EpCAM conjugated HNTs coatings can promote the specific adhesion of CTCs while inhibit the nonspecific adhesion of WBCs. It should

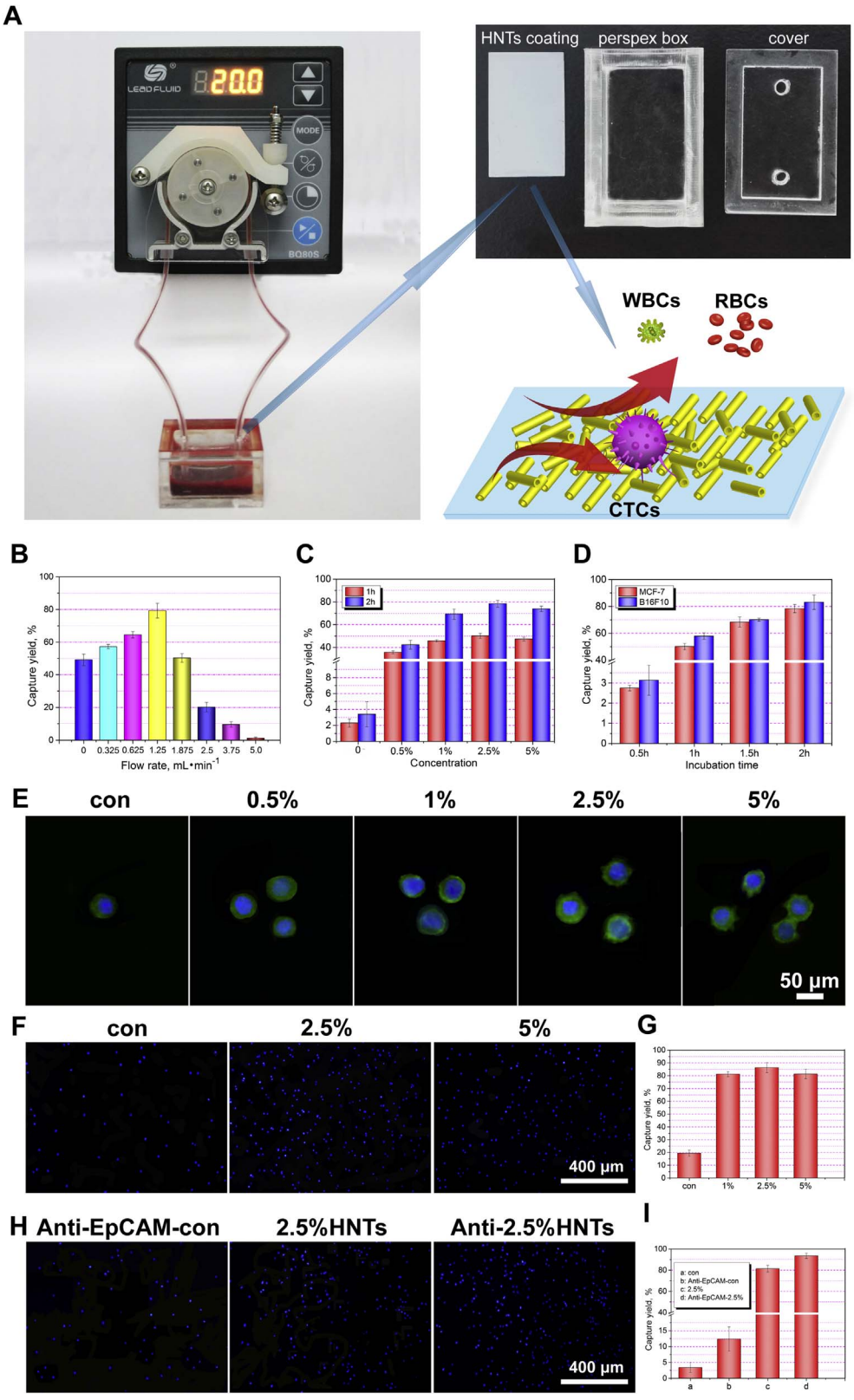

Fig. 7. The photo of a circulating device with a peristaltic pump and the schematic diagram of cell capture from whole blood (A). The capture yield to MCF-7 cells with different flow rate (B). The capture yield to MCF-7 cells with different rough HNTs coating surface (C). The capture yield to MCF-7 cells with different time (D). The Alex Flour 488 and DAPI stained fluorescence microscopy images of captured cells of MCF-7 on the different coatings for 2 h (E). The DAPI stained fluorescence microscopy images showing that the MCF-7 cells captured by different coating surfaces under dynamic shear condition for 1 h and then standing for another 2 h (F) and quantification of the captured MCF-7 (G). The DAPI stained fluorescence microscopy images of the MCF-7 cells captured by smooth glass and 2.5% HNTs coating without and with anti-EpCAM conjugation for 2 h at a flow rate of 1.25 mL·min^{-1} (H) and the cell capture yield (I).

be pointed that the capture ability of the HNTs coatings conjugated with anti-EpCAM under dynamic flow is comparable with the FDA-cleared CELLSEARCH® CTC Test technology which can also capture several to tens of CTCs from 7.5 mL of blood. The high capture ability of HNTs coating towards tumor cells suggests that the device based on HNTs coating exhibits promising application in clinical CTCs capture.

3.4. Killing the capture tumor cells by DOX loaded HNTs coating

HNTs coating conjugated with anti-EpCAM and loaded DOX not only can specifically capture tumor cells but also kill them by the drug effects. The DOX was loaded into HNTs by adsorption before thermal spraying. Fig. 9(A) shows the pure DOX ethanol solution and the HNTs-

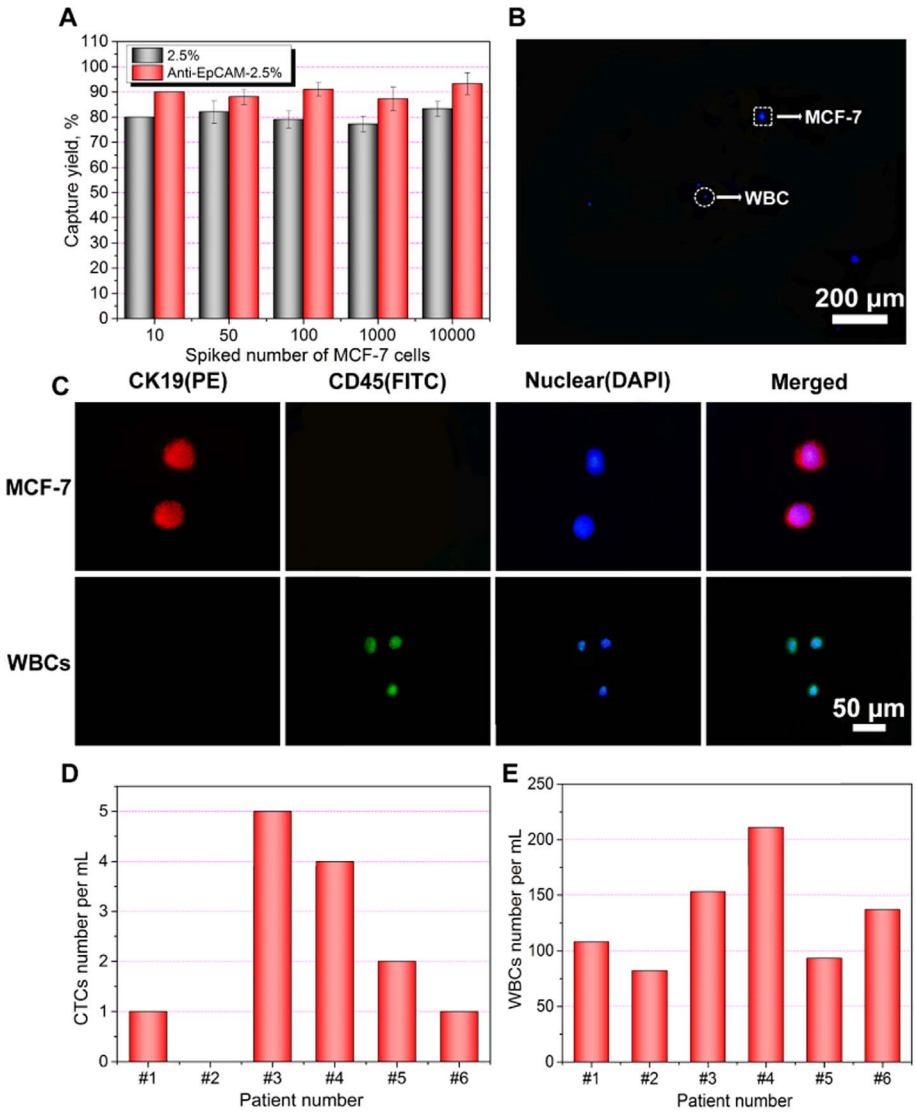

Fig. 8. The capture yield of MCF-7 cells on HNTs coatings with or without anti-EpCAM conjugation for artificial whole blood samples with concentration of 10, 50, 100, 1000 and 10,000 cells·mL^{-1} (n = 3) (A). DAPI stained fluorescence microscopy images of captured cells from artificial whole blood samples by the 2.5% HNTs coating conjugated with anti-EpCAM (B). Three-color immunocytochemistry method for identifying cytokeratin-positive CTCs and CD45-positive WBCs on the HNTs coating conjugated with anti-EpCAM (C). Quantification of CTCs captured from the blood of breast cancer patients (D). Quantification of WBCs captured from the blood of patients with breast cancer (E).

DOX mixture dispersion with similar DOX concentration after centrifugation for 5 min at a rate of 10,000 r/min. The pure DOX ethanol solution is still uniform orange-red, while the upper alcohol becomes clear and transparent in the HNTs-DOX group. The HNTs in the bottom of the centrifuge tube get red, which suggests the DOX is fully loaded into HNTs (loading efficiency is 0.4%). HNTs have unique nanostructure with empty lumen, so DOX can be adsorbed on HNTs by physical absorption [31]. Actually, the DOX loading was also determined using a UV–vis spectrophotometer. The result also confirmed that all the DOX was loaded on HNTs. The loaded DOX in HNTs is expect to be released slowly in blood [64]. Then the HNTs-DOX mixture dispersion was sprayed to uniform drug loaded coating by thermal spraying method. The coating formed from DOX loaded HNTs seems pink in the color (Fig. 9(B). Both the HNTs coating and HNTs-DOX coating were used to capture MCF-7 cell under dynamic shear. After capture, the coatings were rinsed by PBS for 3 times and moved to cell culture plates for following incubation by adding cell culture medium. The cellular activity on the HNTs coating and HNTs-DOX coating tested by CCK-8 colorimetric assay is compared in Fig. 9(C). HNTs are biocompatible clay materials that can be mined from deposits as a raw mineral and are chemically similar to kaolin. Previous studies indicated that HNTs exhibited a high degree of biocompatibility showing no toxicity [65], which makes it perspective for different medical applications. The cell viability of the HNTs group nearly keeps unchanged during the culture period up to 16 h, suggesting high cytocompatibility of HNTs. It can be seen that the cellular viability have not much difference on the two kinds of coatings at the beginning. The relative cellular activity on the HNTs-DOX coating is only 10% lower than that on the raw HNTs coating. However, the cell viability on the raw HNTs coating slightly increases with time, while the cell viability on the HNTs-DOX coating significantly decreases with time. After 4 h, the viability of HNTs-DOX coating groups is lower than 50%. Moreover, the relative cellular activity of the HNTs-DOX coating groups is near to zero after incubation for 16 h. This suggests that HNTs-DOX coating has a strong killing ability towards the captured MCF-7 cells. Cell live/dead staining was further used to detect the viability of tumor cells captured by HNTs coatings with and without DOX at different time (Fig. 9(D). From the fluorescence images of the two groups, the loading DOX into HNTs nearly does not influence the capture efficiency as the similar cell number on the two coating. The MCF-7 cells captured by the raw HNTs coating or DOX loaded HNTs coating surface show negligible differences in viability at the beginning. After 4 h incubation, MCF-7 cells captured on raw HNTs coating surface still display normal morphology with green fluorescence, while some of the MCF-7 cells captured on DOX loaded HNTs coating change into apoptotic state gradually. About half of the MCF-7 cells are red, which suggests DOX released from HNTs can kill the cells. After 8 h, MCF-7 cells captured by raw HNTs coating still display live state, while nearly almost the cells captured by HNTs-

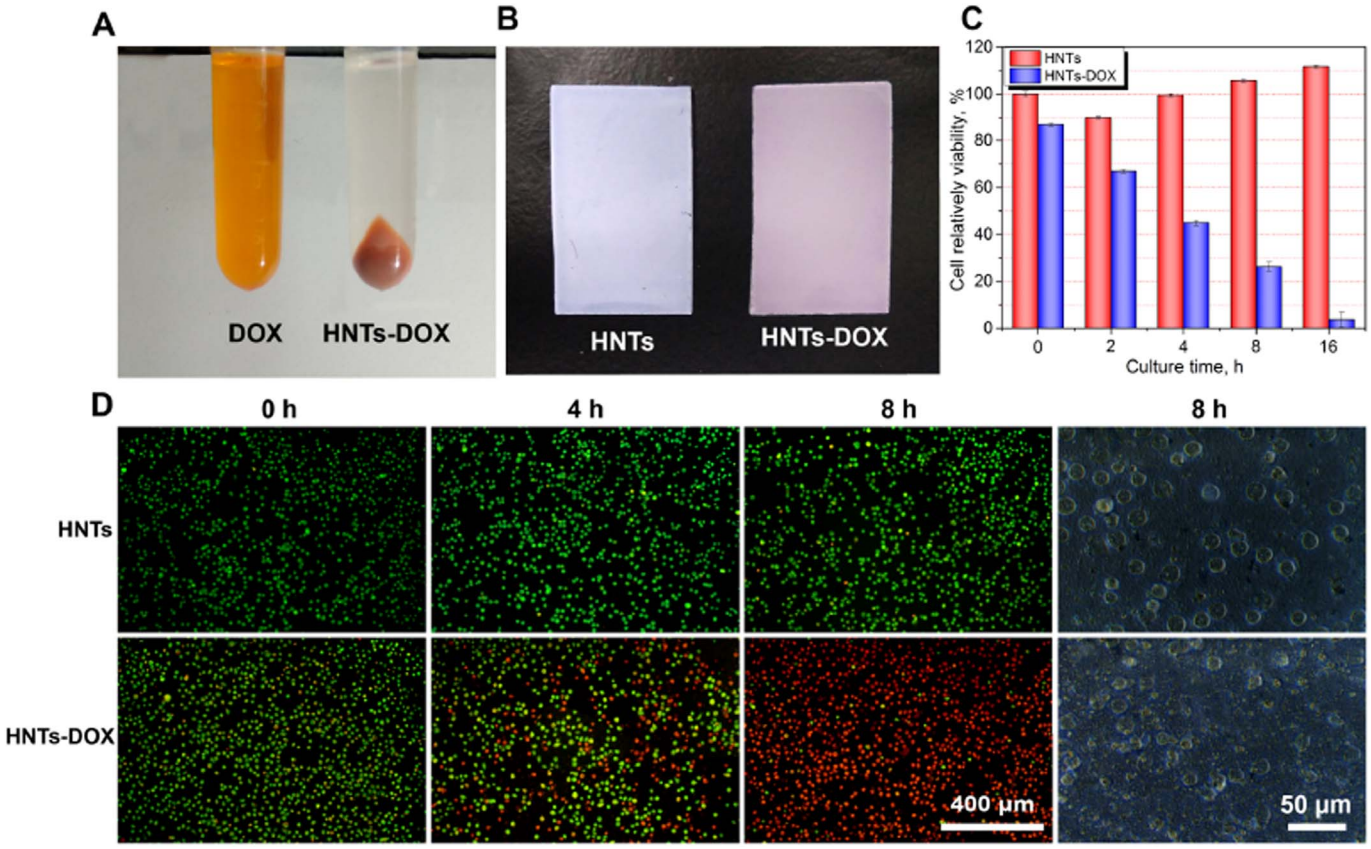

Fig. 9. The photograph of DOX ethyl alcohol solution and HNTs absorbed DOX in ethyl alcohol after centrifuged for 5 min at a rate of 10,000 r/min (A). The photograph of raw HNTs coating and HNTs loaded DOX coating (B). The CCK-8 assay of cell viability for captured MCF-7 cells by the two coatings for different time (C). The AO/EB fluorescence microscopy images and bright field microscopy images of captured MCF-7 cells with different incubation time (D).

DOX coating display significant membrane rupture characteristic of apoptosis. So, the MCF-7 cells captured by the HNTs-DOX coating surface die after 8 h. The morphology result is also consistent with the CCK-8 result. All these results indicate that drug loaded and antibody conjugated HNTs are good systems to prepare rough nanocoating as an implantable device for targeting and killing CTCs in clinic cancer therapy especially for the tumor metastasis.

4. Conclusions

Rough HNTs coating on glass substrate was prepared via thermal spraying of HNTs ethanol dispersion. The surface roughness and thickness of the HNTs coatings increase with the HNTs dispersion concentration. The rough HNTs surfaces show high capture yield for the tumor cells and relatively low capture yield for the normal cells. HNTs rough surface can stimulate tumor cells to produce a large amount of ECM, which is beneficial to the adhesion of tumor cells on HNTs coating. HNTs coating conjugated with anti-EpCAM can improve the capture yield to 93% ± 4% towards to MCF-7 cells. HNTs coating also can specifically capture rare tumor cells from peripheral blood samples and blood samples of patients with metastatic breast cancer. The capture rate and yield can be further improved by providing a suitable dynamic shear condition in a circulating device. Anticancer drug DOX can be effectively loaded into HNTs by adsorption. The HNTs-DOX rough coating conjugated with anti-EpCAM can target and kill CTCs effectively while repelling WBCs. In total, the rough HNTs coatings prepared via a simple thermal spraying method show promising applications in clinical CTCs capture for early diagnosis and monitoring of cancer patients. The drug loaded HNTs coating surfaces also can be designed as an implantable therapeutic device for preventing tumor metastasis.

Acknowledgements

This work was financially supported by National High Technology Research and Development Program of China (2015AA020915), the National Natural Science Foundation of China (51473069 and 51502113), and the Guangdong Natural Science Funds for Distinguished Young Scholar (S2013050014606), Science and Technology Planning Project of Guangdong Province (2014A020217006), Guangdong Special Support Program (2014TQ01C127), the Pearl River S&T Nova Program of Guangzhou (201610010026), and Science and Technology Planning Project of Guangzhou (2017010160233).

References

[1] K. Jakab, C. Norotte, F. Marga, K. Murphy, G. Vunjak-Novakovic, G. Forgacs, Tissue engineering by self-assembly and bio-printing of living cells, Biofabrication 2 (2010) 022001.
[2] V. Kravets, F. Schedin, R. Jalil, L. Britnell, R. Gorbachev, D. Ansell, B. Thackray, K. Novoselov, A. Geim, A.V. Kabashin, Singular phase nano-optics in plasmonic metamaterials for label-free single-molecule detection, Nat. Mater. 12 (2013) 304–309.
[3] S. Huang, X. Fu, Naturally derived materials-based cell and drug delivery systems in skin regeneration, J. Control. Release 142 (2010) 149–159.
[4] A. Verma, F. Stellacci, Effect of surface properties on nanoparticle–cell interactions, Small 6 (2010) 12–21.
[5] K. Balani, R. Anderson, T. Laha, M. Andara, J. Tercero, E. Crumpler, A. Agarwal, Plasma-sprayed carbon nanotube reinforced hydroxyapatite coatings and their interaction with human osteoblasts in vitro, Biomaterials 28 (2007) 618–624.
[6] A.E. Nel, L. Mädler, D. Velegol, T. Xia, E.M. Hoek, P. Somasundaran, F. Klaessig, V. Castranova, M. Thompson, Understanding biophysicochemical interactions at the nano–bio interface, Nat. Mater. 8 (2009) 543–557.
[7] R. Lange, F. Lüthen, U. Beck, J. Rychly, A. Baumann, B. Nebe, Cell-extracellular matrix interaction and physico-chemical characteristics of titanium surfaces depend on the roughness of the material, Biomol. Eng. 19 (2002) 255–261.
[8] C.P. Teng, T. Zhou, E. Ye, S. Liu, L.D. Koh, M. Low, X.J. Loh, K.Y. Win, L. Zhang, M.-

Y. Han, Effective targeted Photothermal ablation of multidrug resistant bacteria and their biofilms with NIR-absorbing gold nanocrosses, Adv. Healthc. Mater. 5 (2016) 2122–2130.
[9] E. Ye, M.D. Regulacio, S.-Y. Zhang, X.J. Loh, M.-Y. Han, Anisotropically branched metal nanostructures, Chem. Soc. Rev. 44 (2015) 6001–6017.
[10] H.J. Yoon, T.H. Kim, Z. Zhang, E. Azizi, T.M. Pham, C. Paoletti, J. Lin, N. Ramnath, M.S. Wicha, D.F. Hayes, Sensitive capture of circulating tumour cells by functionalized graphene oxide nanosheets, Nat. Nanotechnol. 8 (2013) 735–741.
[11] N. Sun, X. Li, Z. Wang, R. Zhang, J. Wang, K. Wang, R. Pei, A multiscale TiO_2 nanorod array for ultrasensitive capture of circulating tumor cells, ACS Appl. Mater. Interfaces 8 (2016) 12638–12643.
[12] H.C. Guo, E. Ye, Z. Li, M.-Y. Han, X.J. Loh, Recent progress of atomic layer deposition on polymeric materials, Mater. Sci. Eng. C 70 (2017) 1182–1191.
[13] W. Wu, X. Wang, X. Liu, F. Zhou, Spray-coated fluorine-free superhydrophobic coatings with easy repairability and applicability, ACS Appl. Mater. Interfaces 1 (2009) 1656–1661.
[14] D.V. Andreeva, D. Fix, H. Möhwald, D.G. Shchukin, Self-healing anticorrosion coatings based on pH-sensitive polyelectrolyte/inhibitor Sandwichlike nanostructures, Adv. Mater. 20 (2008) 2789–2794.
[15] X. Lin, Y. Zeng, X. Zhou, C. Ding, Microstructure of alumina–3wt.% titania coatings by plasma spraying with nanostructured powders, Mater. Sci. Eng. A 357 (2003) 228–234.
[16] V.P. Singh, A. Sil, R. Jayaganthan, A study on sliding and erosive wear behaviour of atmospheric plasma sprayed conventional and nanostructured alumina coatings, Mater. Des. 32 (2011) 584–591.
[17] V.H. Pham, T.V. Cuong, S.H. Hur, E.W. Shin, J.S. Kim, J.S. Chung, E.J. Kim, Fast and simple fabrication of a large transparent chemically-converted graphene film by spray-coating, Carbon 48 (2010) 1945–1951.
[18] I.J. Kramer, J.C. Minor, G. Moreno-Bautista, L. Rollny, P. Kanjanaboos, D. Kopilovic, S.M. Thon, G.H. Carey, K.W. Chou, D. Zhitomirsky, Efficient spray-coated colloidal quantum dot solar cells, Adv. Mater. 27 (2015) 116–121.
[19] E. Ellis, K. Zhang, Q. Lin, E. Ye, A. Poma, G. Battaglia, X.J. Loh, T.-C. Lee, Biocompatible pH-responsive nanoparticles with a core-anchored multilayer shell of triblock copolymers for enhanced cancer therapy, J. Mater. Chem. B 5 (2017) 4421–4425.
[20] Q.Q. Dou, C.P. Teng, E. Ye, X.J. Loh, Effective near-infrared photodynamic therapy assisted by upconversion nanoparticles conjugated with photosensitizers, Int. J. Nanomedicine 10 (2015) 419–432.
[21] C. Dhand, N. Dwivedi, X.J. Loh, A.N. Jie Ying, N.K. Verma, R.W. Beuerman, R. Lakshminarayanan, S. Ramakrishna, Methods and strategies for the synthesis of diverse nanoparticles and their applications: a comprehensive overview, RSC Adv. 5 (2015) 105003–105037.
[22] R. Lakshminarayanan, X.J. Loh, S. Gayathri, S. Sindhu, Y. Banerjee, R.M. Kini, S. Valiyaveettil, Formation of transient amorphous calcium carbonate precursor in quail eggshell mineralization: an in vitro study, Biomacromolecules 7 (2006) 3202–3209.
[23] B.M. Teo, D.J. Young, X.J. Loh, Magnetic anisotropic particles: toward remotely actuated applications, Part. Part. Syst. Charact. 33 (2016) 709–728.
[24] K. Huang, Q. Dou, X.J. Loh, Nanomaterial mediated optogenetics: opportunities and challenges, RSC Adv. 6 (2016) 60896–60906.
[25] Y.M. Lvov, D.G. Shchukin, H. Mohwald, R.R. Price, Halloysite clay nanotubes for controlled release of protective agents, ACS Nano 2 (2008) 814–820.
[26] M. Liu, Z. Jia, D. Jia, C. Zhou, Recent advance in research on halloysite nanotubes-polymer nanocomposite, Prog. Polym. Sci. 39 (2014) 1498–1525.
[27] X.J. Loh, T.-C. Lee, Q. Dou, G.R. Deen, Utilising inorganic nanocarriers for gene delivery, Biomater. Sci. 4 (2016) 70–86.
[28] Q. Dou, X. Fang, S. Jiang, P.L. Chee, T.-C. Lee, X.J. Loh, Multi-functional fluorescent carbon dots with antibacterial and gene delivery properties, RSC Adv. 5 (2015) 46817–46822.
[29] Z. Li, E. Ye, R. David, Lakshminarayanan, X.J. Loh, Recent advances of using hybrid nanocarriers in remotely controlled therapeutic delivery, Small 12 (2016) 4782–4806.
[30] E. Abdullayev, Y. Lvov, Halloysite clay nanotubes as a ceramic “skeleton” for functional biopolymer composites with sustained drug release, J. Mater. Chem. B 1 (2013) 2894–2903.
[31] J. Yang, Y. Wu, Y. Shen, C. Zhou, Y.-F. Li, R.-R. He, M. Liu, Enhanced therapeutic efficacy of doxorubicin for breast cancer using chitosan oligosaccharide-modified Halloysite nanotubes, ACS Appl. Mater. Interfaces 8 (2016) 26578–26590.
[32] H. Wu, Y. Shi, C. Huang, Y. Zhang, J. Wu, H. Shen, N. Jia, Multifunctional nanocarrier based on clay nanotubes for efficient intracellular siRNA delivery and gene silencing, J. Biomater. Appl. 28 (2014) 1180–1189.
[33] R. Zhai, B. Zhang, L. Liu, Y. Xie, H. Zhang, J. Liu, Immobilization of enzyme biocatalyst on natural halloysite nanotubes, Catal. Commun. 12 (2010) 259–263.
[34] C. Chao, J. Liu, J. Wang, Y. Zhang, B. Zhang, Y. Zhang, X. Xiang, R. Chen, Surface modification of halloysite nanotubes with dopamine for enzyme immobilization, ACS Appl. Mat, Interfaces 5 (2013) 10559–10564.
[35] M. Liu, C. Wu, Y. Jiao, S. Xiong, C. Zhou, Chitosan–halloysite nanotubes nanocomposite scaffolds for tissue engineering, J. Mater. Chem. B 1 (2013) 2078–2089.
[36] M. Liu, L. Dai, H. Shi, S. Xiong, C. Zhou, In vitro evaluation of alginate/halloysite nanotube composite scaffolds for tissue engineering, Mater. Sci. Eng. C 49 (2015) 700–712.
[37] M. Liu, Y. Shen, P. Ao, L. Dai, Z. Liu, C. Zhou, The improvement of hemostatic and wound healing property of chitosan by halloysite nanotubes, RSC Adv. 4 (2014) 23540–23553.
[38] M. Alavi, A. Totonchi, M.A. Okhovat, M. Motazedian, P. Rezaei, M. Atefi, The effect of a new impregnated gauze containing bentonite and halloysite minerals on blood coagulation and wound healing, Blood Coagul. Fibrinolysis 25 (2014) 856–859.
[39] D.G. Shchukin, G.B. Sukhorukov, R.R. Price, Y.M. Lvov, Halloysite nanotubes as biomimetic nanoreactors, Small 1 (2005) 510–513.
[40] A.D. Hughes, M.R. King, Use of naturally occurring halloysite nanotubes for enhanced capture of flowing cells, Langmuir 26 (2010) 12155–12164.
[41] M.J. Mitchell, C.A. Castellanos, M.R. King, Immobilized surfactant-nanotube complexes support selectin-mediated capture of viable circulating tumor cells in the absence of capture antibodies, J. Biomed. Mater. Res. A 103 (2015) 3407–3418.
[42] M.J. Mitchell, C.A. Castellanos, M.R. King, Surfactant functionalization induces robust, differential adhesion of tumor cells and blood cells to charged nanotube-coated biomaterials under flow, Biomaterials 56 (2015) 179–186.
[43] M. Liu, R. He, J. Yang, W. Zhao, C. Zhou, Stripe-like clay nanotubes patterns in glass capillary tubes for capture of tumor cells, ACS Appl. Mater. Interfaces 8 (2016) 7709–7719.
[44] H. Xu, Z.P. Aguilar, L. Yang, M. Kuang, H. Duan, Y. Xiong, H. Wei, A. Wang, Antibody conjugated magnetic iron oxide nanoparticles for cancer cell separation in fresh whole blood, Biomaterials 32 (2011) 9758–9765.
[45] A.D. Hughes, J. Mattison, L.T. Western, J.D. Powderly, B.T. Greene, M.R. King, Microtube device for selectin-mediated capture of viable circulating tumor cells from blood, Clin. Chem. 58 (2012) 846–853.
[46] B. Wang, A.L. Weldon, P. Kumnorkaew, B. Xu, J.F. Gilchrist, X. Cheng, Effect of surface nanotopography on immunoaffinity cell capture in microfluidic devices, Langmuir 27 (2011) 11229–11237.
[47] E. Ye, X.J. Loh, Polymeric hydrogels and nanoparticles: a merging and emerging field, Aust. J. Chem. 66 (2013) 997–1007.
[48] A. Ranella, M. Barberoglou, S. Bakogianni, C. Fotakis, E. Stratakis, Tuning cell adhesion by controlling the roughness and wettability of 3D micro/nano silicon structures, Acta Biomater. 6 (2010) 2711–2720.
[49] S.P. Khan, G.G. Auner, G.M. Newaz, Influence of nanoscale surface roughness on neural cell attachment on silicon, Nanomedicine 1 (2005) 125–129.
[50] W. Chen, S. Weng, F. Zhang, S. Allen, X. Li, L. Bao, R.H. Lam, J.A. Macoska, S.D. Merajver, J. Fu, Nanoroughened surfaces for efficient capture of circulating tumor cells without using capture antibodies, ACS Nano 7 (2012) 566–575.
[51] Y. Wan, Y. Wang, Z. Liu, X. Qu, B. Han, J. Bei, S. Wang, Adhesion and proliferation of OCT-1 osteoblast-like cells on micro-and nano-scale topography structured poly (ι-lactide), Biomaterials 26 (2005) 4453–4459.
[52] J. Rosales-Leal, M. Rodríguez-Valverde, G. Mazzaglia, P. Ramon-Torregrosa, L. Diaz-Rodriguez, O. Garcia-Martinez, M. Vallecillo-Capilla, C. Ruiz, M. Cabrerizo-Vilchez, Effect of roughness, wettability and morphology of engineered titanium surfaces on osteoblast-like cell adhesion, Colloids Surf. A Physicochem. Eng. Asp. 365 (2010) 222–229.
[53] M.M. Burger, A difference in the architecture of the surface membrane of normal and virally transformed cells, Proc. Natl. Acad. Sci. 62 (1969) 994–1001.
[54] G.B. Kolata, Microvilli: a major difference between normal and cancer cells? Science 188 (1975) 819–820.
[55] K. Das, S. Bose, A. Bandyopadhyay, Surface modifications and cell–materials interactions with anodized Ti, Acta Biomater. 3 (2007) 573–585.
[56] H.-C. Flemming, J. Wingender, The biofilm matrix, nature reviews, Microbiology 8 (2010) 623–633.
[57] S.L. Stott, R.J. Lee, S. Nagrath, M. Yu, D.T. Miyamoto, L. Ulkus, E.J. Inserra, M. Ulman, S. Springer, Z. Nakamura, Isolation and characterization of circulating tumor cells from patients with localized and metastatic prostate cancer, Sci. Transl. Med. 2 (2010) (25ra23-25ra23).
[58] H. Lu, L.Y. Koo, W.M. Wang, D.A. Lauffenburger, L.G. Griffith, K.F. Jensen, Microfluidic shear devices for quantitative analysis of cell adhesion, Anal. Chem. 76 (2004) 5257–5264.
[59] S. Nagrath, L.V. Sequist, S. Maheswaran, D.W. Bell, D. Irimia, L. Ulkus, M.R. Smith, E.L. Kwak, S. Digumarthy, A. Muzikansky, Isolation of rare circulating tumour cells in cancer patients by microchip technology, Nature 450 (2007) 1235–1239.
[60] H.J. Yoon, A. Shanker, Y. Wang, M. Kozminsky, Q. Jin, N. Palanisamy, M.L. Burness, E. Azizi, D.M. Simeone, M.S. Wicha, Tunable thermal-sensitive polymer–graphene oxide composite for efficient capture and release of viable circulating tumor cells, Adv. Mater. 28 (2016) 4891–4897.
[61] R.D. Goldman, S. Khuon, Y.H. Chou, P. Opal, P.M. Steinert, The function of intermediate filaments in cell shape and cytoskeletal integrity, J. Cell Biol. 134 (1996) 971–983.
[62] S. Wang, K. Liu, J. Liu, Z.T.F. Yu, X. Xu, L. Zhao, T. Lee, E.K. Lee, J. Reiss, Y.K. Lee, Highly efficient capture of circulating tumor cells by using nanostructured silicon substrates with integrated chaotic micromixers, Angew. Chem. Int. Ed. 50 (2011) 3084–3088.
[63] X. Liu, L. Chen, H. Liu, G. Yang, P. Zhang, D. Han, S. Wang, L. Jiang, Bio-inspired soft polystyrene nanotube substrate for rapid and highly efficient breast cancer-cell capture, NPG Asia Mater. 5 (2013) e63.
[64] J. Yang, Y. Wu, Y. Shen, C. Zhou, Y.F. Li, R.R. He, M. Liu, Enhanced therapeutic efficacy of doxorubicin for breast cancer using chitosan oligosaccharide-modified Halloysite nanotubes, ACS Appl. Mat. Interfaces 8 (2016) 26578.
[65] Y. Lvov, E. Abdullayev, Functional polymer–clay nanotube composites with sustained release of chemical agents, Prog. Polym. Sci. 38 (2013) 1690–1719.